arXiv:1608.04400v3 [physics.flu-dyn] 5 Apr 2017

New smoothed particle hydrodynamics (SPH) formulation for modeling heat conduction with solidification and melting

Amirsaman Farrokhpanah*[1], Markus Bussmann[1], and Javad Mostaghimi[1]

[1]*Department of Mechanical & Industrial Engineering, University of Toronto*

April 7, 2017

Abstract

When modelling phase change, the latent heat released (absorbed) during solidification (melting) must be included in the heat transfer equation. In this paper, different SPH methods for the implementation of latent heat, in the context of transient heat conduction, are derived and tested. First, SPH discretizations of two finite element methods are presented, but these prove to be computationally expensive. Then, by starting from a simple approximation and enhancing accuracy using different numerical treatments, a new SPH method is introduced, that is fast and easy to implement. An evaluation of this new method on various analytical and numerical results confirms its accuracy and robustness.

Keywords: Smoothed Particle Hydrodynamics, Heat conduction, Solidification, Melting

1 Introduction

Heat transfer and phase change are of importance in many engineering applications, e.g. coating surfaces with paint or metal, freezing and thawing of food products, and the casting of plastics and metals. There are a wide range of methods available for numerical prediction of transient phase change problems. Knowledge of the solid-liquid front position is of key importance. In many numerical methods for phase change, the effect of latent heat is added as a source term to the heat transfer equation, like the methods of Passandideh Fard [1] and Voller [2], or by modifying the heat capacity coefficient, as in Thomas et al. [3], Hsiao [4], and Dalhuijsen et al. [5].

The finite volume method was first used for the study of phase change heat transfer, followed by finite element methods. This transition was due to the flexibility of the finite

*farrokh@mie.utoronto.ca

element method for complex boundary conditions and implementations [5]. In this paper, a Smoothed Particle Hydrodynamics method (SPH), or in a more general sense, integral interpolations are investigated for phase change processes. SPH is a Lagrangian mesh-free CFD method introduced in 1977 by Lucy [6] and Gingold and Monaghan [7], and was initially applied to astrophysics. Since 1977, many studies have been conducted on the accuracy and applicability of SPH to various fluid problems [8]. Tsunami simulations [9], simulations of floating bodies like ships [10], and multiphase flow studies [11, 12, 13] are all examples of SPH applications. The main advantage of SPH is its ability to handle complex geometries. The implementation of different boundary conditions in SPH is also straightforward. Moreover, SPH codes are easily parallelized.

Several studies have attempted to solve phase change problems using SPH. Cleary et al. [14, 15] focused on the explicit inclusion of latent heat after solving the enthalpy form of the heat conduction equation. This method has been used to model casting [16] and solidification of molten metal drops impacting a surface [17, 18, 19]. Monaghan et al. [20] modelled the solidification of pure and binary alloys, where phase change was simulated by removing liquid particles and transferring their mass to a stationary grid of solid particles. The drawback of this method is the need for virtual particles, which results in a doubling of the number of particles inside the domain, and makes the method computationally expensive and difficult to implement into available solvers.

In this study, a new SPH formulation, using integral interpolations is introduced for modelling transient heat conduction with phase change. Application of the method to various available analytical and numerical results demonstrates the robustness of the method. Compared to other effective heat capacity implementations, this method is fast and yet more accurate.

2 Incorporation of Latent Heat into an Effective Heat Capacity

2.1 Governing Equations

Transient heat conduction is mathematically represented as

$$\frac{\partial H}{\partial t} = \nabla \cdot (k \nabla T) \tag{1}$$

By expressing H as a function of T, equation 1 can be written as

$$\frac{dH}{dT}\frac{\partial T}{\partial t} = \nabla \cdot (k \nabla T) \tag{2}$$

In this form, equation 2 does not account for the release (absorption) of latent heat during solidification (melting). To do that, the parameter

$$C = \frac{dH}{dT} \tag{3}$$

known as the effective heat capacity, can be modified to include the effect of latent heat, as follows [21, 22]

$$C = \begin{cases} C_s & T < T_m \\ C_m + L\delta(T - T_m) & T = T_m \\ C_l & T > T_m \end{cases} \tag{4}$$

where $\delta(T - T_m)$ the Dirac delta function. It can be easily confirmed that using this form of C yields a total heat release of $\int_{-\infty}^{\infty} L\delta(T - T_m)dT = L$.

2.2 Numerical Implementations of Latent Heat Release

First, SPH discretizations of two finite element methods for solving equation 1 are presented. Then, by starting with a simple approximation, new SPH interpolations for the inclusion of latent heat via equation 4 are derived. This leads to five different methods, that are presented in this paper as equations 6, 7, 13, 14, and 17.

2.2.1 Variational Methods

A first approach is to use the variation of enthalpy as a function of temperature to calculate the value of C using equation 3. The first equation presented here was developed by Del Diudice et al. [23] by transforming equation 3 using the direction of the temperature gradient, s, as [5]

$$C = \frac{\partial H/\partial s}{\partial T/\partial s} = \frac{(\partial H/\partial x)l_{sx} + (\partial H/\partial y)l_{sy} + (\partial H/\partial z)l_{sz}}{\partial T/\partial s} \tag{5}$$

with direction cosines defined as $l_{s\alpha} = \frac{\partial T}{\partial \alpha}/\frac{\partial T}{\partial s}$ and $\frac{\partial T}{\partial s} = \sqrt{(\frac{\partial T}{\partial x})^2 + (\frac{\partial T}{\partial y})^2 + (\frac{\partial T}{\partial z})^2}$. This gives an effective heat capacity

$$C = \frac{(\partial H/\partial x)(\partial T/\partial x) + (\partial H/\partial y)(\partial T/\partial y) + (\partial H/\partial z)(\partial T/\partial z)}{(\partial T/\partial x)^2 + (\partial T/\partial y)^2 + (\partial T/\partial z)^2} \tag{6}$$

Another approach is similar to that of Lemmon [24], where s is taken as the normal direction of the interface, and yields

$$C = \left[\frac{(\partial H/\partial x)^2 + (\partial H/\partial y)^2 + (\partial H/\partial z)^2}{(\partial T/\partial x)^2 + (\partial T/\partial y)^2 + (\partial T/\partial z)^2}\right]^{1/2} \tag{7}$$

These two equations were implemented in a finite element context by Thomas et al. [3] and Dalhuijsen et al. [5]. To discretize equations 6 and 7 for SPH, an approach inspired by Del Giudice et al. [23] is used here. In their finite element method, the enthalpy is smoothed by a shape function before using the above equations. Here, the value of enthalpy for each SPH particle is calculated from its temperature using [5]

$$C = \begin{cases} \int_{T_{ref}}^{T} \rho C_s(T)dT & T < T_1 \\ \int_{T_{ref}}^{T_1} \rho C_s(T)dT + \int_{T_1}^{T} \rho\left(dL/dT + C_m(T)\right)dT & T_1 \le T \le T_2 \\ \int_{T_{ref}}^{T_1} \rho C_s(T)dT + \rho L + \int_{T_1}^{T_2} \rho C_m(T)dT + \int_{T_2}^{T} \rho C_l(T)dT & T > T_2 \end{cases} \tag{8}$$

To increase accuracy and stability, we propose that the value of enthalpy at each particle is smoothed using

$$H_i^s = \sum_j \frac{m_j}{\rho_j} H_j W^P(\boldsymbol{x_j} - \boldsymbol{x_i}, h) \tag{9}$$

With the value of enthalpy known, the gradients of enthalpy that appear in equations 6 and 7 can be calculated using

$$(\nabla H)_i = \sum_j \frac{m_j}{\rho_j} \left[H_j^s - H_i^s\right] \boldsymbol{\nabla W^P}(\boldsymbol{x_j} - \boldsymbol{x_i}, h) \tag{10}$$

A similar formulation is used to calculate the first gradient of temperature. The second gradient of temperature that appears in these equations is calculated by taking the gradient of the first gradient:

$$\left(\nabla^2 T\right)_i = \rho_i \sum_j m_j \left[\frac{\boldsymbol{\nabla T}_j}{\rho_j^2} + \frac{\boldsymbol{\nabla T}_i}{\rho_i^2}\right] \cdot \boldsymbol{\nabla W^P}(\boldsymbol{x_j} - \boldsymbol{x_i}, h) \tag{11}$$

2.2.2 Step Release

Calculation of the partial derivatives appearing in equations 6 and 7 demands many computational steps, and so motivates the search for alternative methods. Returning to equation 4, it is convenient to replace δ, that releases latent heat at a single temperature T_m, with a function that releases the latent heat over a finite temperature interval around T_m. Hsiao [4] shows that a very simple substitute for δ is of the form

$$C = \begin{cases} C_s & T < T_m - \Delta T \\ C_m + \frac{L}{2\Delta T} & T_m - \Delta T \leq T \leq T_m + \Delta T \\ C_l & T > T_m + \Delta T \end{cases} \tag{12}$$

Here the total latent heat released over the interval of $2\Delta T$ is still L. Figure 1 shows this step jump in the apparent heat capacity.

The main drawback of this approach is the need for a phase change temperature interval. For some particles during a simulation, the value of temperature may jump from a value above this interval to a value below it in one time step [4]. This means that the effect of latent heat might be bypassed if the temperature variation in a time step is large compared to ΔT, and imposes a limitation on the solution time step [5]. Additionally, for the case of pure materials where solidification/melting occurs at a single temperature, the artificial phase change interval [3] has no physical meaning. A poor choice of this interval may cause solution inaccuracy.

For the phase change of alloys with a mushy zone, where solidification/melting occurs over a temperature range, equation 12 becomes

$$C = \begin{cases} C_s & T \leq T_1 \\ C_m + \frac{L}{T_2 - T_1} & T_1 < T < T_2 \\ C_l & T \geq T_2 \end{cases} \tag{13}$$

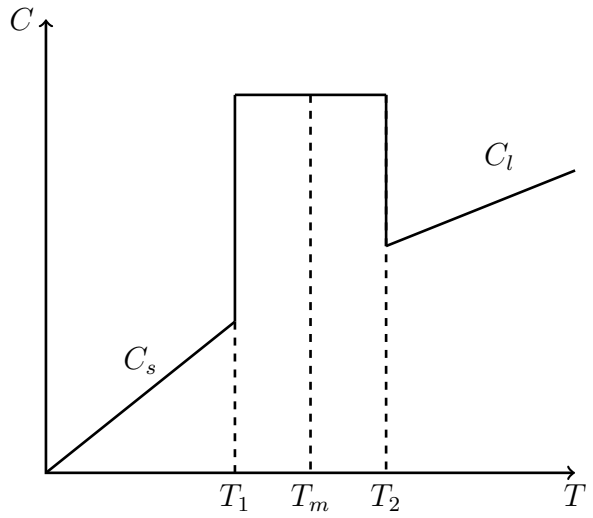

Figure 1: Apparent heat capacity with a step jump for the latent heat.

2.2.3 Gradual Release

A second approach is to replace the Dirac delta function δ by an even smoothing function W that has the identity property of δ, $\int_{-\infty}^{\infty} W(T - T_m, h^*)dT = 1$, and is defined over a temperature range, shown here as $\Delta T = k^* \times h^*$. The integer k^* and the float h^* are similar in definition to the usual SPH notations of k and h, the only difference being that k and h are defined in the space domain and are based on particle positioning, while k^* and h^* are defined over the temperature domain of particles. In other words, where the value of $k \times h$ determines a radius around each particle within which its neighbours contribute to a heat transfer calculation, similarly, $k^* \times h^*$ defines a radius in the one dimensional domain of temperature around the melting temperature. This new radius acts as a second filter in addition to $k \times h$. In formulations where both filters are present, the only particles that contribute to heat transfer are those close to a certain particle in both the space and temperature domains.

Replacing δ with the smoothing function W, depending on the choice of W, has been shown to have a second or higher order of accuracy [25]. Figure 2 demonstrates the smoothing function. More detailed discussions on the derivation of a SPH formulation, and more general integral interpolations, can be found in [26, 27]. Using this definition, equation 4 can be rewritten as

$$C = \begin{cases} C_s & T < T_m - \Delta T \\ C_m + LW^T(T - T_m, h^*) & T_m - \Delta T \leq T \leq T_m + \Delta T \\ C_l & T > T_m + \Delta T \end{cases} \tag{14}$$

where W^T is a 1D kernel defined in the temperature domain.

2.2.4 Smoothed Gradual Release

The accuracy and efficiency of equation 14 can be further improved by smoothing the term $LW^T(T - T_m, h^*)$ with a higher order kernel [28, 29]. This is achieved using the standard

SPH interpolation [30]

$$f(x_0) \cong -\sum_{j=1}^{N} \frac{m_j}{\rho_j} f(x_j) W(x_i - x_0, h) \tag{15}$$

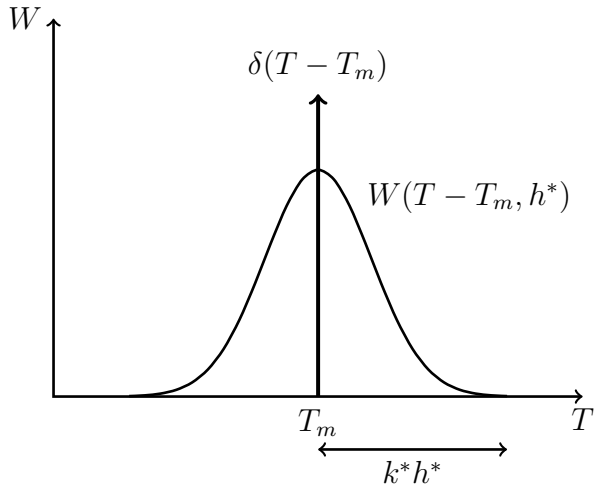

Figure 2: The smoothing function W.

Summation here is performed over all j particles located in the neighbourhood radius of particle i. With this definition, the latent heat in equation 14 at the position of an arbitrary particle i is smoothed using

$$L_i^s = \sum_{j=1}^{N} \frac{m_j}{\rho_j} [L W^T(T_j - T_m, h^*)] W^P(\boldsymbol{x_j} - \boldsymbol{x_i}, h) \tag{16}$$

and hence equation 4 can be rewritten as

$$C = \begin{cases} C_s & T < T_m - \Delta T \\ C_m + L^s & T_m - \Delta T \leq T \leq T_m + \Delta T \\ C_l & T > T_m + \Delta T \end{cases} \tag{17}$$

ΔT is identical to the radius of influence of the smoothing function, $W^T(T - T_m, h^*)$. In this formulation, the latent heat is distributed to particles based on the difference between the particle temperature and the melting temperature, and also based on how far other particles in its neighbourhood are from the reference melting temperature. In other words, this equation accounts for two variations: 1) changes in temperature of each particle with respect to the melting point, and 2) the variation of temperature in the domain with respect to the position vector $\boldsymbol{x}$. The term $LW^T(T_j - T_m, h^*)$ is a discretization of $L\delta$ and a function of temperature only. Furthermore, temperature itself is a function of particle position in the domain $T = T(x)$. The second term, $W^P(\boldsymbol{x_j} - \boldsymbol{x_i}, h)$, accounts for the change of temperature with respect to position. The smoothing behaviour of equation 16 assures there is no sudden jump in enthalpy within the domain with respect to changes in the position vector $\boldsymbol{x}$.

3 Results and Discussion

We now present the results of a series of tests of the five methods, referred to as equations 6, 7, 13, 14, and 17.

3.1 Two-Dimensional Problem: Phase Change in the Corner of a Square

The first test case is of solidification in the corner of a square initially filled with fluid, as shown in figure 3. The cuboid is assumed long enough in the z direction to form a 2D problem at its cross-section. For the solution here, a 3D setup of the domain has been used with a periodic boundary condition in the z direction. Solidification starts as the temperature of all side walls is suddenly changed to a value below the freezing point. From the analytical solution of this problem [31, 32], the solid-liquid interface that moves from the corner toward the square centre is of the form

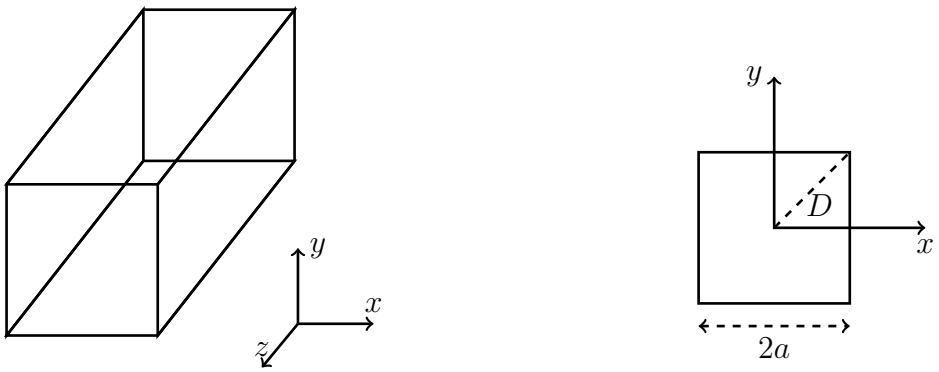

Figure 3: Problem description: fluid is assumed to be inside a Cuboid which is infinitely long in z direction. At the start of simulation, temperature at walls is suddenly dropped to a value below freezing temperature.

$$f(x^*) = [\lambda^m + C/(x^{*m} - \lambda^m)]^{1/m} \tag{18}$$

where $x^* = x/(4\alpha t)^{1/2}$, and λ is calculated by solving

$$\frac{e^{-\lambda^2}}{erf\lambda} - \frac{T_i^* e^{-\lambda^2}}{erfc\lambda} = \sqrt{\pi}\beta\lambda \tag{19}$$

where $T_i^* = k_l/k_s(T_i - T_m)/(T_m - T_w)$ and $\beta = 1/St$. Values of m and C depend on the non-dimensional parameters T_i and β. For β=0.25 and T_i^*=0.3, these values are $\lambda = 0.708$, $C = 0.159$ and $m = 5.02$ [31]. The non-dimensional position of the solidification front on the cuboid diagonal (D in figure 3) can be also calculated from equation 18. On the diagonal, $f(x^*) = x^*$. Solving equation 18 for this equality results in $f(x^*) = 0.8958$.

Numerically, SPH particles are uniformly distributed in all directions. Figure 4 shows the particle distribution at any $x - y$ cross-section. Since each particle has a neighbourhood radius of $3\Delta x$, three layers of particles are placed in the wall so that all inner particles have

a complete neighbourhood (filled circles in figure 4). The temperature of all wall particles is kept constant throughout the simulation. Properties of the solid and liquid are assumed to remain constant in each phase. Density is assumed to be the same in the two phases.

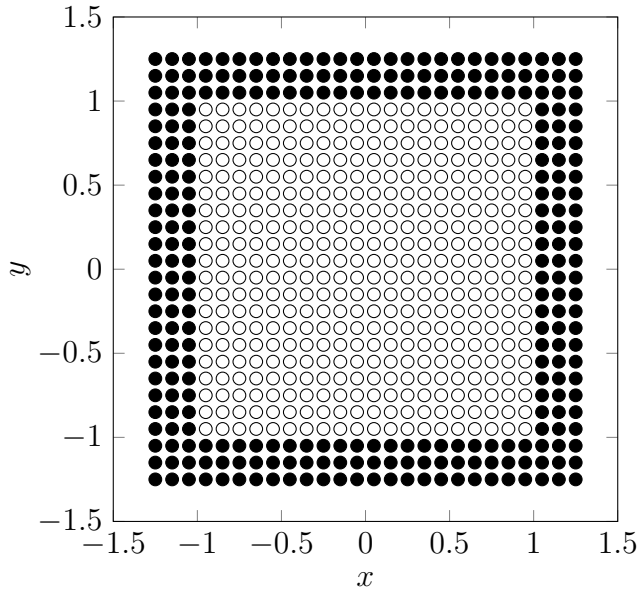

Figure 4: Initial particle positioning. Hollow circles show fluid particle positions, while filled circles indicate wall particles.

A comparison of numerical tests using each of the five equations versus the analytical solution is shown in figure 5. The error values are calculated by comparing the numerical solidification front position on the diagonal against the analytical value of 0.8958 using $\left|\frac{\bar{x}^* - 0.8958}{0.8958} \times 100\right|$.

Results demonstrate that equations 6, 7, 13, and 14 yield nearly identical large errors, while the most accurate results are obtained using equation 17.

3.1.1 Comparison to Numerical Results

To compare the five equations against available numerical results, the solidification in the corner region is solved for the following non-dimensional parameters: $\theta = (T_i - T_w)/(T_m - T_w) = 9/7$, $St = C_s(T_m - T_w)/L = 2$, $\alpha_l/\alpha_s = 0.9$, and $k_l/k_s = 0.9$. The tests conducted here have a fine particle resolution of 100×100 particles in the $x - y$ cross-section. Results for this case are plotted in figure 6. Numerical results of the same problem from Cao et al. [33], Hsiao et al. [4], and Keung [34] using a coarser mesh of 20×20 are also shown. All methods converge to the same solution.

3.1.2 Effect of particle resolution

To assess mesh dependency, the previous problem is solved on a much coarser 30×30 mesh. Results are shown in figure 7 along with the same results of Hsiao et al. [4], Cao et al. [33], and Keung [34] with a mesh resolution of 20×20. It is clear that by reducing the resolution,

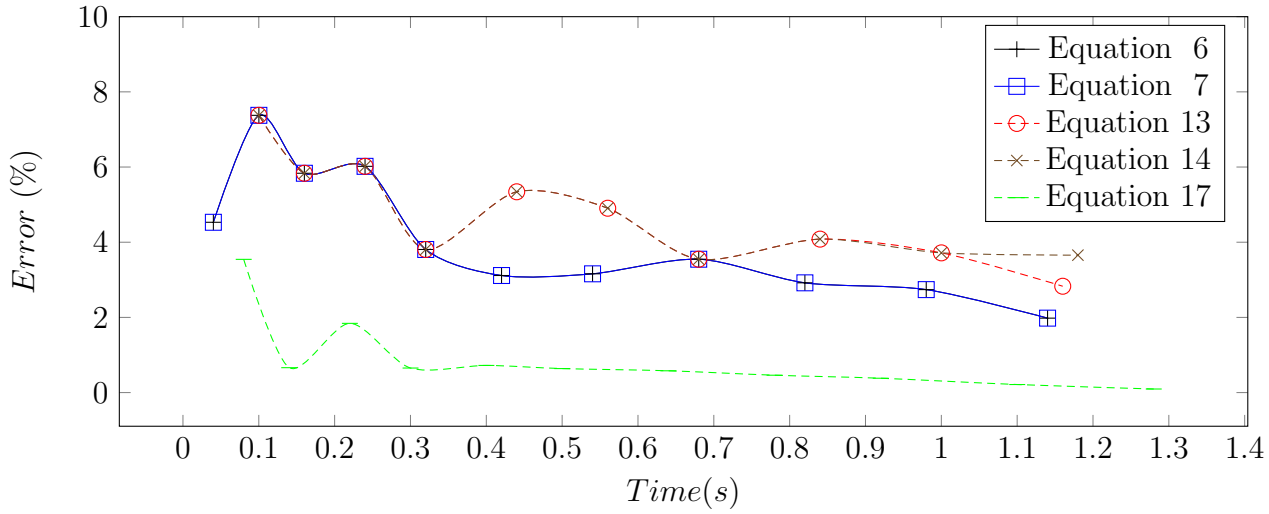

Figure 5: Solidification front position versus the analytical solution, for solidification in a corner.

equations 13 and 14 start to deviate from the converged values, while equations 6, 7, and 17 show near to no sensitivity to this decrease in solution resolution. This shows how these equations are more accurate at coarser resolutions.

As figure 5 shows that equation 17 is the most accurate, the rest of this section is focused on further examination of the functionality of this equation.

Figure 8 illustrates the melting of a cuboid, for $\theta = 0.3, St = 4$, $\alpha_l/\alpha_s = 1$, and $k_l/k_s = 1$. Results are compared at two resolutions, 40×40 and 100×100, at 0.1, 0.4, 0.8, 1.2, and 1.44 seconds (figure 8). The solid lines in this figure show the analytical solution.

3.1.3 Effect of ΔT

Equation 17 assumes that phase change occurs over a temperature range ΔT, the value of which must be chosen for each problem. It was mentioned previously that the value of ΔT must be small enough to approximate physical reality, yet if ΔT is too small, some particles might not experience phase change as the temperature can jump from a value above (below) melting to a value below (above) in one time step during solidification (melting). This must be taken into consideration when choosing ΔT and Δt. For the previous test cases, a dimensionless value of $\Delta T = 0.02$ was used.

The melting cuboid problem is considered again, with $T_i^* = 0.3, St = 4$, $\alpha_l/\alpha_s = 1$, and $k_l/k_s = 1$. ΔT is set to values of 0.00001, 0.01, 0.02, 0.05, and 0.08. The error values for this test case, compared to the analytical solution, are plotted in figure 9. For very small ΔT (0.00001 here), errors are large as many particles do not experience the latent heat, and at large ΔT (0.08 here), the error grows as the phase change temperature interval deviates too far from the physical reality. The results of various test cases, including the one reported here, confirm that there exists a large range of ΔT over which the results are relatively independent of the choice of ΔT.

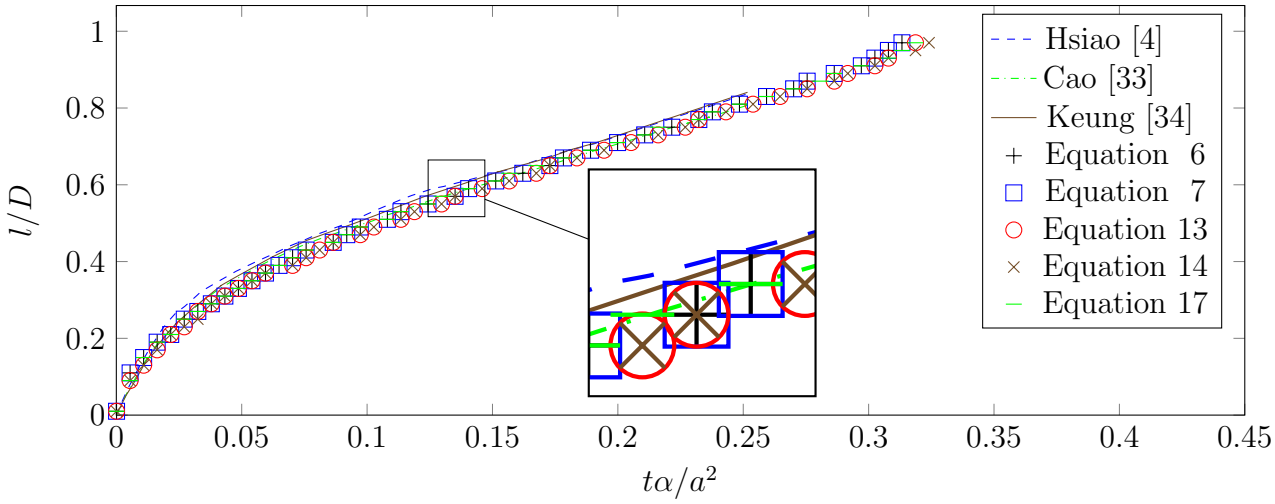

Figure 6: Position of the solidification front on the diagonal cross section of the cuboid (resolution: 100×100)

3.1.4 Effect of Smoothing Kernel

Finally, the choice of smoothing kernel that appears in equation 16 is important as it dictates how the latent heat is released into the domain. Table 1 lists three smoothing functions (from [35, 36, 37]). These kernels are plotted in figure 10. To compare these kernels, W^T and W^P are taken to be identical, where the former is in the 1D domain of temperature and the latter is in the 3D $x-y-z$ domain. This only changes the constant coefficients of these kernels. For instance, the Meng [35] kernel in 3D has a coefficient of $21/(16\pi h^3)$ for W^P and a coefficient of $3/4h$ (in 1D) for W^T. Note that the α^{3D} values are used for the 2D test case here, since it is solved in a 3D domain.

Table 1: Smoothing kernels

Kernel	α^{3D}	α^{1D}	Ref
$W(R,h) = \alpha \begin{cases} (1-R/2)^4(2R+1) & 0 \le R \le 2 \\ 0 & otherwise \end{cases}$	$\frac{21}{16\pi h^3}$	$\frac{3}{4h}$	[35]
$W(R,h) = \alpha \begin{cases} (3/16)R^2 - (3/4)R + 3/4 & 0 \le R \le 2 \\ 0 & otherwise \end{cases}$	$\frac{5}{4\pi h^3}$	$\frac{1}{h}$	[36]
$W(R,h) = \alpha \begin{cases} 2/3 - R^2 + R^3/2 & 0 \le R < 1 \\ (1/6)(2-R)^3 & 1 \le R < 2 \\ 0 & otherwise \end{cases}$	$\frac{3}{2\pi h^3}$	$\frac{1}{h}$	[37]

For the case of the solidification of the cuboid, results using these three kernels are compared to the analytical solution. Figure 11 shows that all three kernels produce accurate

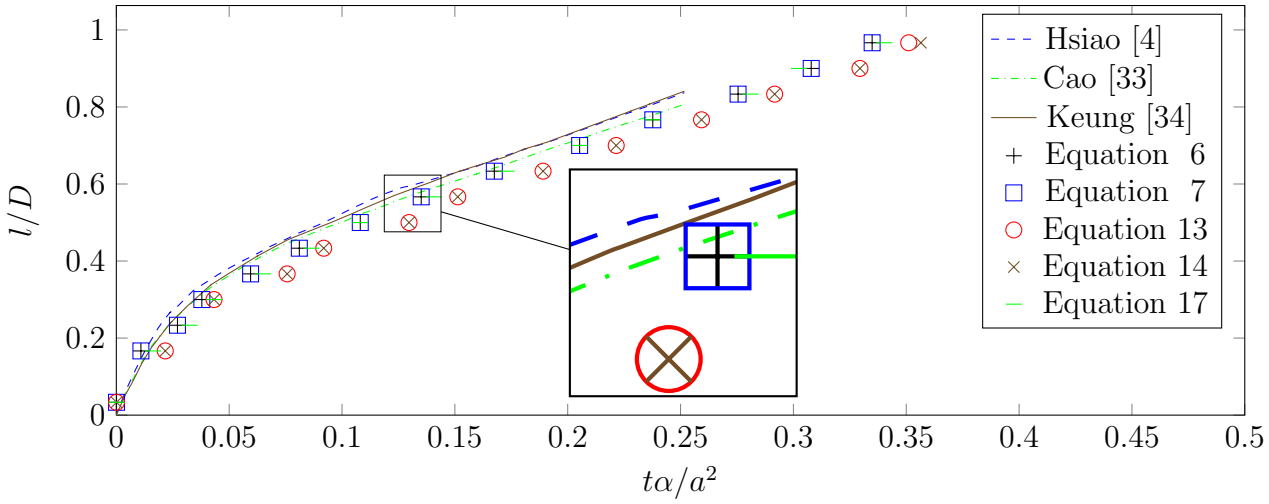

Figure 7: Position of the melting front moving along the diagonal of a cuboid (30×30)

results with an error below 5%, but the Meng et al. [35] and Johnson et al. [36] kernels produce somewhat more accurate solutions.

3.2 Three-Dimensional Problems

In this section, the validity of the model of equation 17 is assessed on two 3D test cases.

3.2.1 Melting of a sphere

The first 3D test case is the melting of a sphere. Problem specifications are the same as in [38]. A sphere is considered to be initially at its melting temperature ($T_i = 0°C$). At time 0, the temperature of the wall surrounding the sphere is raised to a value higher than the melting temperature ($T_w = 1°C$). In this test case, similar to the test performed by [38], the Stefan number St is varied from 1 to 4. The sphere has a radius of $0.25m$ and specific heats and thermal diffusivities are set to unity. Figure 12 shows the total melting time for the sphere at different Stefan numbers. The melting times obtained using equation 17, as can be seen in figure 12, are in good agreement with the mathematical model of [39].

Particle temperatures for the case of $St = 4$ are plotted in figure 13 at $t = 0, 0.0025$, and 0.0065.

3.2.2 Melting of a cone

The second 3D test is the melting of a cone. For comparison, the problem specifications have been chosen similar to a test case from [40]. A cone with a half angle of 30 degrees is initially at $T_i = 0°C$. The temperature on the wall surrounding the cone is increased to $T_w = 0.3°C$ at $t = 0$. The phase change interface at different times is shown in figure 14, and compared to the results of Ayasoufi et al. [40] (CE/SE method). As can be seen, the SPH solution yields results close to those of [40], while slightly underpredicting the melt front.

3.3 Computational Cost

Finally, the SPH solver used here was developed to run entirely on graphics processing units (GPU). The device used for this study is the NVIDIA® Tesla® K20 GPU accelerator with 2496 processor cores and a processor core clock of 706 MHz. For the sample conduction problems with phase change, 10.3 kB of memory per particle was needed on the GPU device. The five equations mentioned before perform quite consistently with regard to the amount of computational time, except for equation 13, which is near 8% faster than the rest. This is because equation 13 approximates the amount of latent heat released (absorbed) without the need of smoothing steps or evaluating gradients. However, equation 13 is also the least accurate. Of the rest of the equations, equation 17 requires the least number of computation steps, and so is easier to implement.

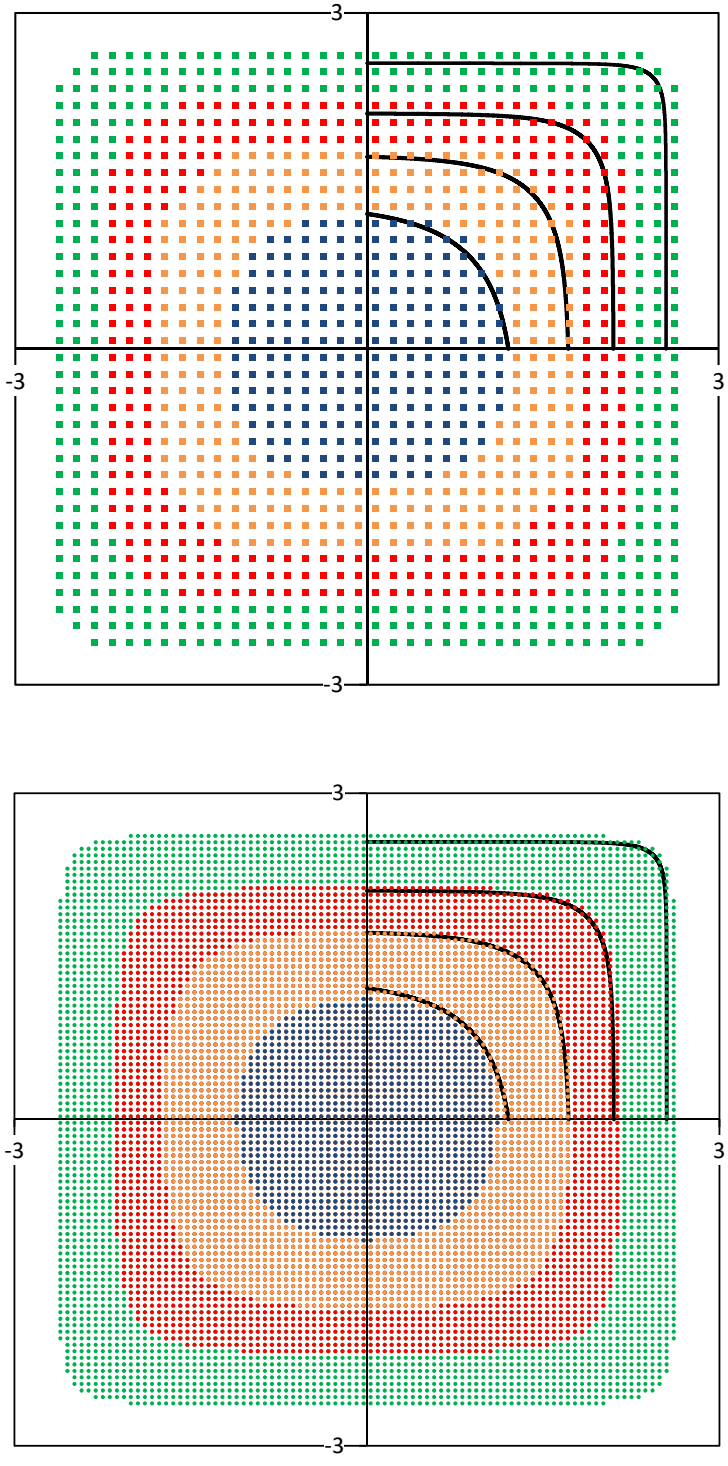

Figure 8: Melting of a cuboid at 0.1, 0.4, 0.8, 1.2, and 1.44 seconds. Solid lines are the analytical solution. Solution resolution: 40×40 (top) and 100×100 (bottom).

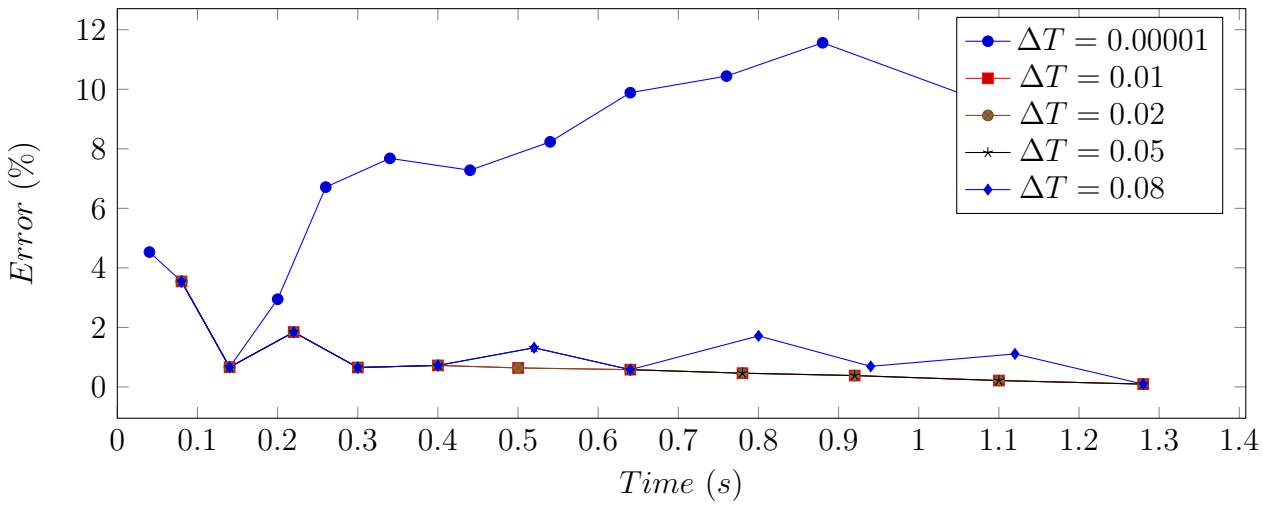

Figure 9: Error of the solidification front position versus the analytical solution, for solidification in a corner, for various ΔT.

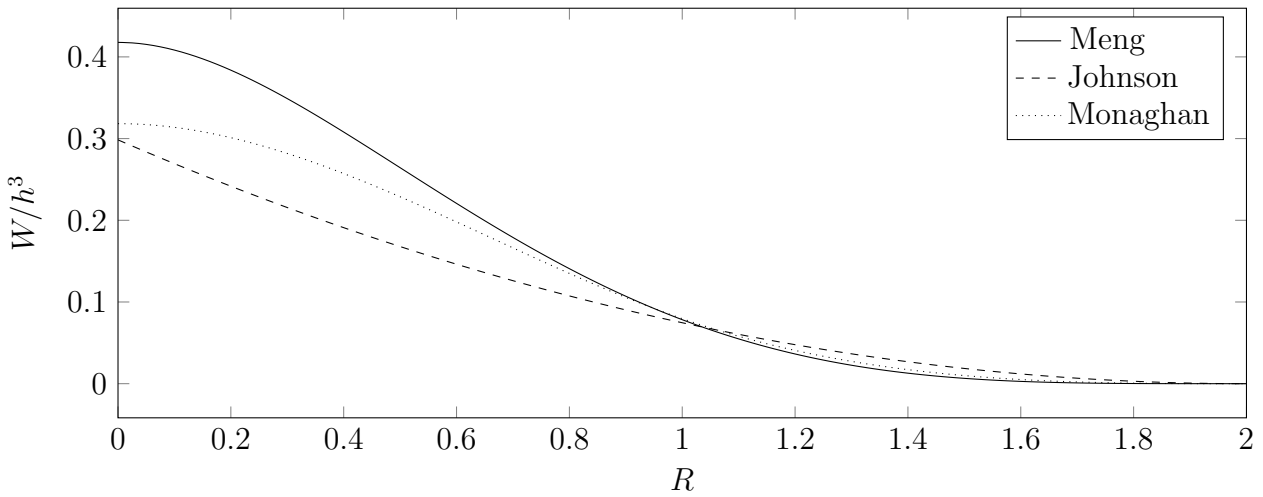

Figure 10: $W(R,h)/h^3$ for the three smoothing kernels.

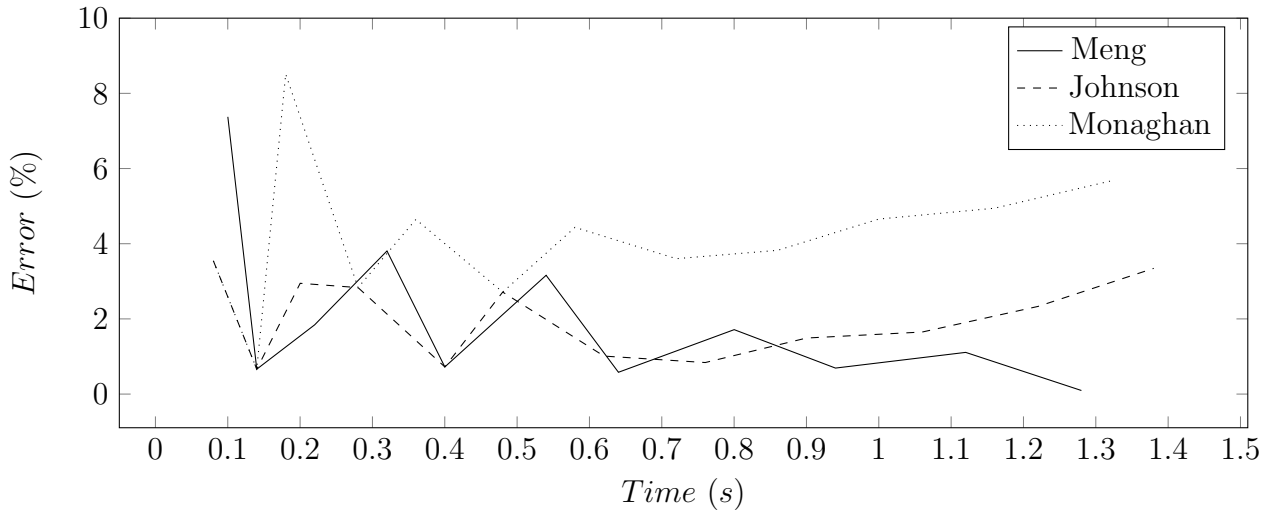

Figure 11: Error of the solidification front position versus the analytical solution, for three different kernels.

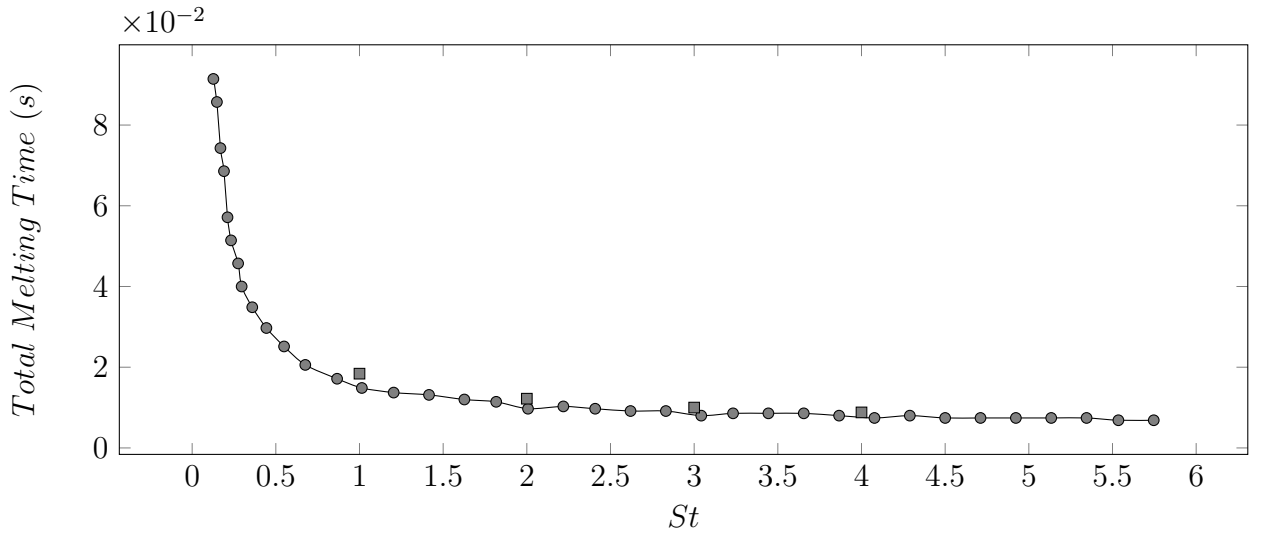

Figure 12: Melting of a sphere. Total time of melting versus Stefan number. Squares show results obtained using the model presented here, and the solid line is from the mathematical model of [39].

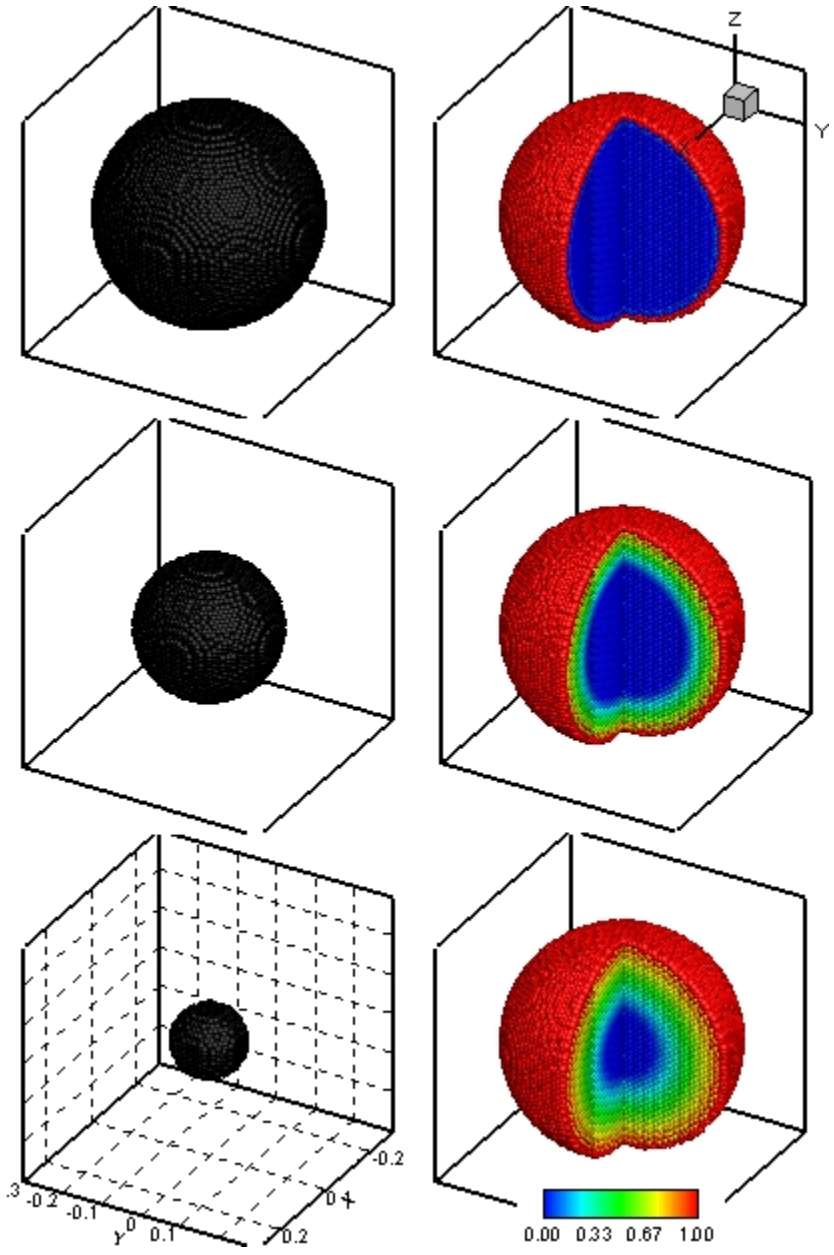

Figure 13: Melting of a sphere of radius 0.25, with a wall temperature $T_w = 1°C$, at $t = 0, 0.0025$, and 0.0065 seconds. Left: un-melted particles; Right: temperature.

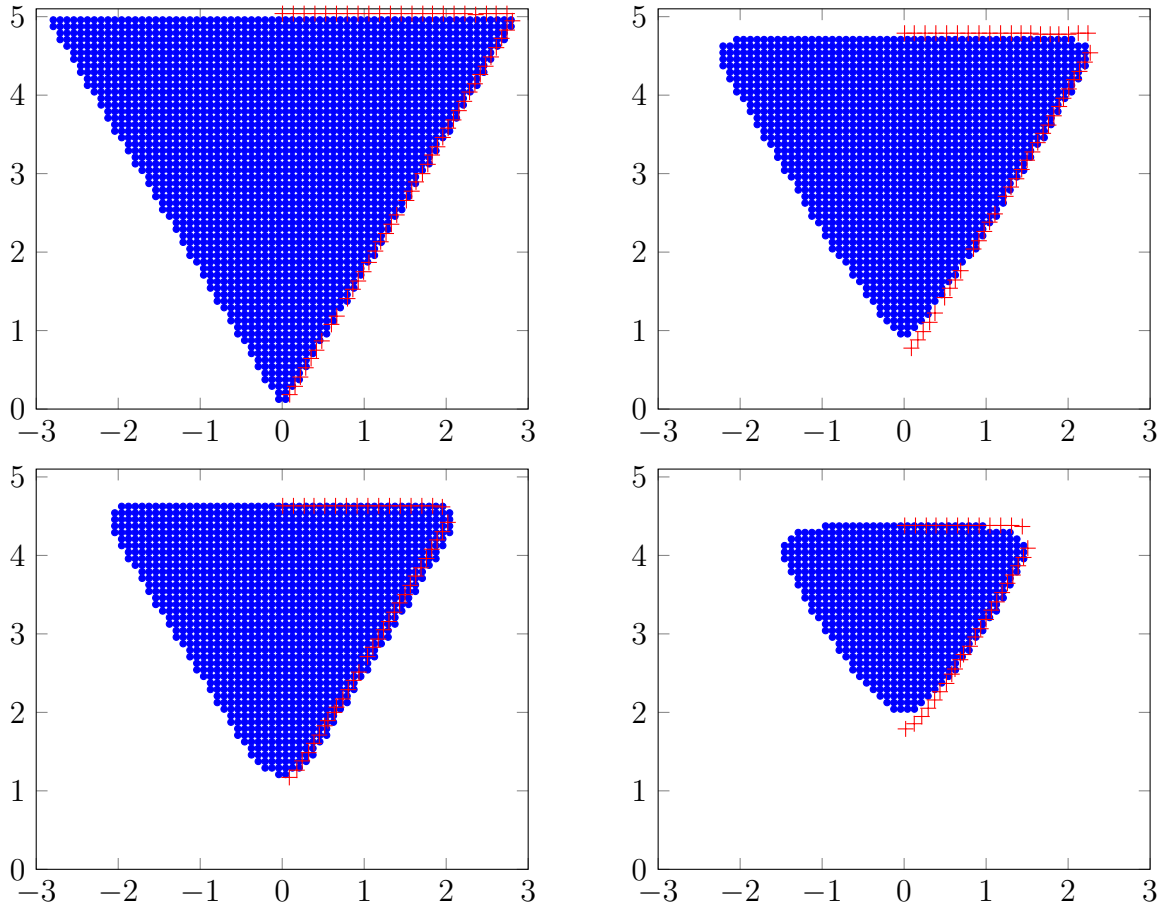

Figure 14: Melting of a cone. Interface position is plotted at different times: 0.05, 0.1, 0.25, and 0.5. Red crosses are the results of Ayasoufi et al. [40] obtained using a space-time conservation element and solution element (CE/SE) method.

4 Conclusions

Modelling conduction heat transfer with phase change in SPH has been investigated. The release/absorption of latent heat during phase change is accounted for by modifying the heat capacity in the energy equation. A new approach is introduced, which uses smoothing and superposition of two kernels to gradually release/absorb the latent heat near the phase change temperature. Compared to a number of alternatives, this new approach yields accurate solutions while limiting the computational cost. The approximations proposed here, although based on a SPH formulation, are also applicable to grid-based methods.

References

[1] M. Passandideh Fard, J. Mostaghimi, Droplet impact and solidification in a thermal spray process: droplet-substrate interactions, in: Proceedings of the 9th National Thermal Spray Conference, 1996.

[2] V. R. Voller, C. Prakash, A fixed grid numerical modelling methodology for convection-diffusion mushy region phase-change problems, International Journal of Heat and Mass Transfer 30 (8) (1987) 1709–1719.

[3] B. Thomas, I. Samarasekera, J. Brimacombe, Comparison of numerical modeling techniques for complex, two-dimensional, transient heat-conduction problems, Metallurgical Transactions B 15 (2) (1984) 307–318.

[4] J. Hsiao, B. T. Chung, An efficient algorithm for finite element solution to two-dimensional heat transfer with melting and freezing, Journal of Heat Transfer 108 (2) (1986) 462–464.

[5] A. Dalhuijsen, A. Segal, Comparison of finite element techniques for solidification problems, International Journal for Numerical Methods in Engineering 23 (10) (1986) 1807–1829.

[6] L. B. Lucy, A numerical approach to the testing of the fission hypothesis, The Astronomical Journal 82 (1977) 1013–1024.

[7] R. A. Gingold, J. J. Monaghan, Smoothed particle hydrodynamics: theory and application to non-spherical stars, Monthly Notices of the Royal Astronomical Society 181 (3) (1977) 375–389.

[8] J. P. Morris, P. J. Fox, Y. Zhu, Modeling low Reynolds number incompressible flows using SPH, Journal of Computational Physics 136 (1) (1997) 214 – 226.

[9] P. L.-F. Liu, H. H.-J. Yeh, C. Synolakis (Eds.), Advanced numerical models for simulating tsunami waves and runup, Advances in Coastal and Ocean Engineering, World Scientific, 2008.

[10] B. Cartwright, P. Groenenboom, D. McGuckin, Examples of ship motion and wash predictions by smoothed particle hydrodynamics (SPH), in: 9th Symposium on Practical Design of Ships and Other Floating Structures, Luebeck-Travemuende, Germany, 2004.

[11] X. Hu, N. Adams, A multi-phase SPH method for macroscopic and mesoscopic flows, Journal of Computational Physics 213 (2) (2006) 844–861.

[12] N. Grenier, D. Touze, M. Antuono, A. Colagrossi, An improved SPH method for multiphase simulations, in: 8th International Conference on Hydrodynamics, ICHD, 2008.

[13] A. M. Tartakovsky, K. F. Ferris, P. Meakin, Lagrangian particle model for multiphase flows, Computer Physics Communications 180 (10) (2009) 1874–1881.

[14] P. Cleary, J. Ha, J. Mooney, V. Ahuja, Effect of heat transfer and solidification on high pressure die casting, in: Proc. 13th Australasian Fluid Mechanics Conference, Melbourne, 1998, pp. 679–682.

[15] P. Cleary, J. Ha, M. Prakash, T. Nguyen, 3D SPH flow predictions and validation for high pressure die casting of automotive components, Applied Mathematical Modelling 30 (11) (2006) 1406–1427.

[16] P. W. Cleary, Extension of SPH to predict feeding, freezing and defect creation in low pressure die casting, Applied Mathematical Modelling 34 (11) (2010) 3189–3201.

[17] M. Zhang, H. Zhang, L. Zheng, Application of smoothed particle hydrodynamics method to free surface and solidification problems, Numerical Heat Transfer, Part A: Applications 52 (4) (2007) 299–314.

[18] M. Zhang, H. Zhang, L. Zheng, Simulation of droplet spreading, splashing and solidification using smoothed particle hydrodynamics method, International Journal of Heat and Mass Transfer 51 (13) (2008) 3410–3419.

[19] M. Zhang, H. Zhang, L. Zheng, Numerical investigation of substrate melting and deformation during thermal spray coating by SPH method, Plasma Chemistry and Plasma Processing 29 (1) (2009) 55–68.

[20] J. J. Monaghan, H. E. Huppert, M. G. Worster, Solidification using smoothed particle hydrodynamics, Journal of Computational Physics 206 (2) (2005) 684–705.

[21] C. Bonacina, G. Comini, A. Fasano, M. Primicerio, Numerical solution of phase-change problems, International Journal of Heat and Mass Transfer 16 (10) (1973) 1825–1832.

[22] J.-S. Hsiao, Numerical and analytical analysis of heat transfer with ablation in a two-dimensional region, Ph.D. thesis, University of Akron (1983).

[23] S. Del Giudice, G. Comini, R. Lewis, Finite element simulation of freezing processes in soils, International Journal for Numerical and Analytical Methods in Geomechanics 2 (3) (1978) 223–235.

[24] E. C. Lemmon, Phase-change techniques for finite element conduction codes, Tech. Rep. CONF-790710-2, Idaho National Engineering Lab., Idaho Falls (USA) (1979).

[25] G.-R. Liu, M. B. Liu, Smoothed particle hydrodynamics: a meshfree particle method, World Scientific, 2003.

[26] A. Farrokhpanah, B. Samareh, J. Mostaghimi, Applying contact angle to a two-dimensional multiphase smoothed particle hydrodynamics model, Journal of Fluids Engineering 137 (4) (2015) 041303.

[27] A. Farrokhpanah, Applying contact angle to a two-dimensional smoothed particle hydrodynamics (SPH) model on a graphics processing unit (GPU) platform, Master's thesis, University of Toronto (2012).

[28] I. Aleinov, E. Puckett, Computing surface tension with high-order kernels, in: Proceedings of the 6th International Symposium on Computational Fluid Dynamics, Lake Tahoe, CA, 1995, pp. 4–8.

[29] M. Rudman, A volume-tracking method for incompressible multifluid flows with large density variations, International Journal for Numerical Methods in Fluids 28 (2) (1998) 357–378.

[30] J. P. Morris, Simulating surface tension with smoothed particle hydrodynamics, International Journal for Numerical Methods in Fluids 33 (3) (2000) 333–353.

[31] K. A. Rathjen, L. M. Jiji, Heat conduction with melting or freezing in a corner, Journal of Heat Transfer 93 (1) (1971) 101–109.

[32] H. Budhia, F. Kreith, Heat transfer with melting or freezing in a wedge, International Journal of Heat and Mass Transfer 16 (1) (1973) 195–211.

[33] Y. Cao, A. Faghri, W. S. Chang, A numerical analysis of Stefan problems for generalized multi-dimensional phase-change structures using the enthalpy transforming model, International Journal of Heat and Mass Transfer 32 (7) (1989) 1289–1298.

[34] C.-S. Keung, The use of sources and sinks in solving two-dimensional heat conduction problems with change of phase in arbitrary domains, Ph.D. thesis, Columbia University, New York, NY. (1980).

[35] S. Meng, R. Yang, J.-S. Wu, H. Zhang, Simulation of droplet spreading on porous substrates using smoothed particle hydrodynamics, International Journal of Heat and Mass Transfer 77 (2014) 828–833.

[36] G. R. Johnson, R. A. Stryk, S. R. Beissel, SPH for high velocity impact computations, Computer Methods in Applied Mechanics and Engineering 139 (1) (1996) 347–373.

[37] J. J. Monaghan, J. C. Lattanzio, A refined particle method for astrophysical problems, Astronomy and Astrophysics 149 (1985) 135–143.

[38] A. Ayasoufi, T. G. Keith, R. K. Rahmani, Application of the conservation element and solution element method in numerical modeling of three-dimensional heat conduction with melting and/or freezing, Journal of Heat Transfer 126 (6) (2004) 937–945.

[39] V. Alexiades, Mathematical modeling of melting and freezing processes, CRC Press, 1992.

[40] A. Ayasoufi, T. Keith, Application of the conservation element and solution element method in numerical modeling of heat conduction with melting and/or freezing, International Journal of Numerical Methods for Heat & Fluid Flow 13 (4) (2003) 448–472.